

Supplementary Information

Tunable index metamaterials made by bottom-up approaches

Mayte Gómez-Castaño,^{1,2} Hanbin Zheng,¹ Juan Luis García-Pomar,² Renaud Vallée,¹ Agustín Mihi,^{*2} and Serge Ravaine^{*1}

¹Centre de Recherche Paul Pascal, CNRS, University of Bordeaux, UMR 5031, F-33600 Pessac, France

²Institute of Materials Science of Barcelona (ICMAB-CSIC), UAB Campus, 08193 Bellaterra, Spain

*Correspondence to amihi@icmab.es and ravaine@crpp-bordeaux.cnrs.fr

Contents

1. Effect of the dielectric refractive index of the spheres
2. Fabrication process of double fishnet metamaterials
3. Experimental divergence from simulations
4. Electromagnetic spatial profiles after the multilayered electrodeposition
5. Effective parameters retrieval of bianisotropic metamaterials
6. Negative refraction in a metamaterial prism
7. Angle dependence of the operation wavelength
8. Comparison between the experimental response and Fresnel modelling
9. Gap and diameter dependence of the negative refractive index

1. Effect of the dielectric refractive index of the spheres

Equivalently to the diameter of the beads and the gap width between the metallic layers, the dielectric index of the spheres n_d can affect the effective refractive index n of the metamaterial. Fig. S1 compares three simulated cases of a double fishnet structure where n_d acquires values of three typical polymers such as polystyrene ($n_d = 1.59$), polyethylene ($n_d = 1.55$) and polyamide ($n_d = 1.50$). As can be observed, the reduction in n_d leads to a blue shift of the real part of n while slightly increasing its negative value. This shift can be understood from the typical relation between the resonance of a metallic system and the surrounding dielectric medium, where higher dielectric indices give rise to a redshift of the operation wavelength.

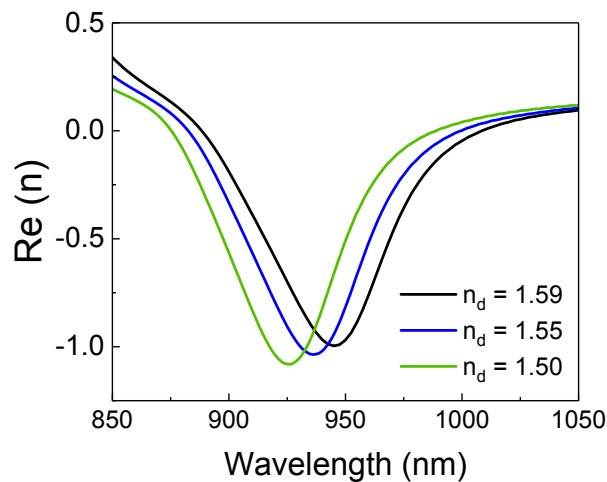


Fig. S1. Real part of the effective refractive index of the metamaterial when varying the dielectric index of the spheres. The main features of the structure are two 50 nm thick Au layers separated by a 25 nm wide air gap and perforated by 200 nm large spheres, with a lattice parameter of 480 nm.

2. Fabrication process of double fishnet metamaterials

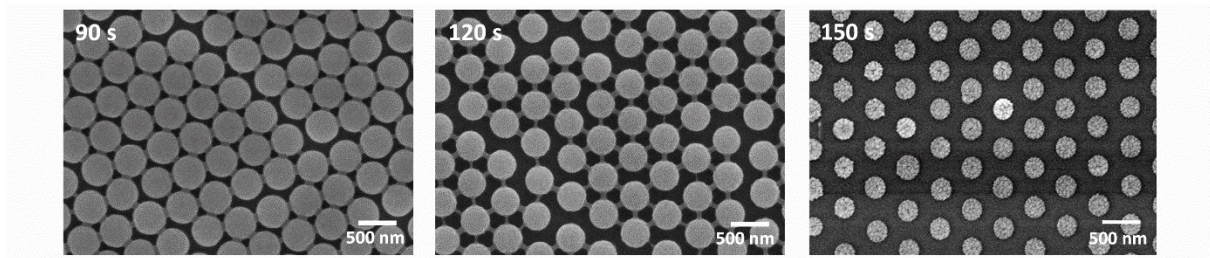


Fig. S2. SEM images of non-close-packed monolayers of PS beads after reduction of their diameter by oxygen plasma for different etching times of 90, 120 and 150 s.

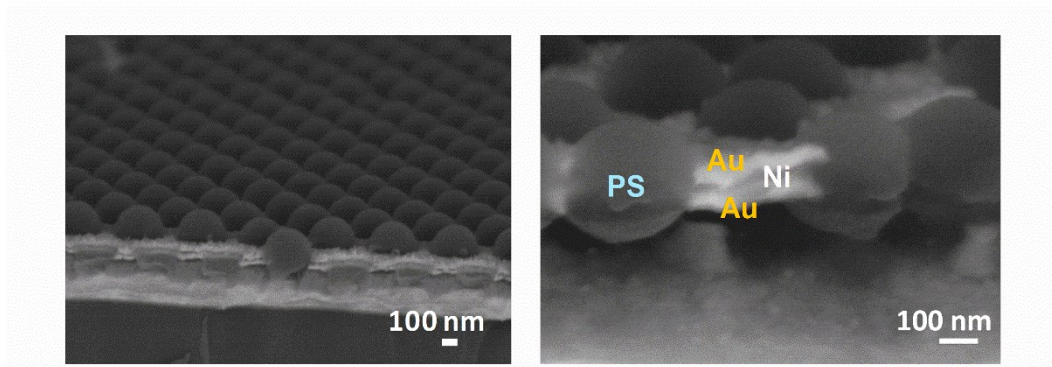


Fig. S3. SEM images of a multilayered nanostructure composed by etched spheres of $D = 340$ nm, two 50 nm thick Au layers symmetrically placed regarding the monolayer axis and a 70 nm thick Ni spacer.

3. Experimental divergence from simulations

The small discrepancies between measured and calculated spectra of Fig. 4 of the main text can be explained with further simulations that reproduce more accurately our experimental systems.

In Fig. 4b, the broader experimental dip shown around 660 nm can be understood as a slight inhomogeneity of the particles size D . This is evidenced by averaging the simulated spectra obtained from multiple diameters covering the error range provided in the manuscript (270 ± 20 nm). As a consequence of this averaging, the small dip appearing at around 570 nm of the simulated spectrum disappears as well, as shown in Fig. S4a.

Regarding the missing dip around 430 nm in the simulation as compared to the experiment in Fig. 4d, we attribute the disagreement to our experimental set up. On one hand, in the simulated spectrum,

the excitation of the structures was performed with a normally incident wave. On the other hand, the measured reflectivity was acquired by both exciting and collecting the signal through an objective with a numerical aperture of 0.2, which involves the excitation and detection of light impinging with angles in the range 0 - 12°. Fig. S4b illustrates a better agreement between the experimental spectrum and the averaged simulated spectra, obtained for angles of incidence ranging from 0 to 10°.

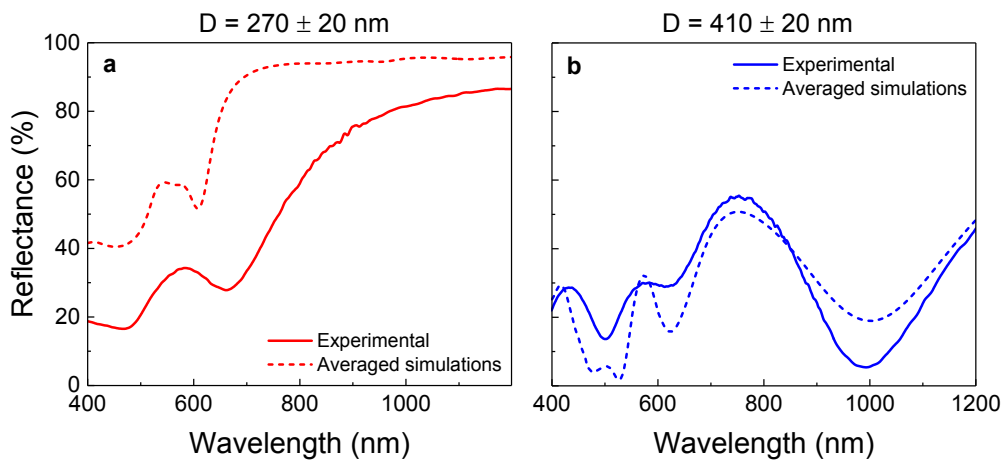


Fig. S4 Measurements (solid lines) and averaged simulations (dashed lines) of reflectance for Au-Ni-Au films embedded with particles of diameter D . The simulated curves correspond to an average over (a) the error range of D and (b) angles of incidence ranging from 0 to 10°.

4. Electromagnetic spatial profiles after the multilayered electrodeposition

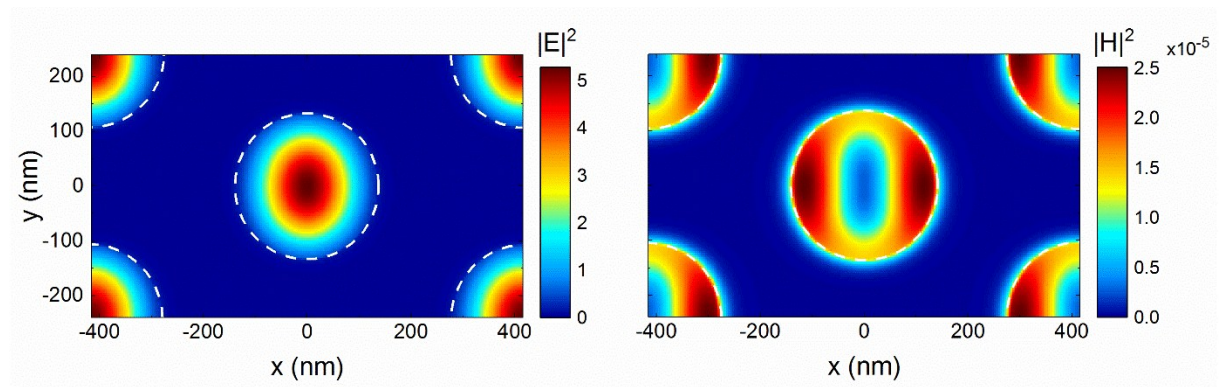


Fig. S5. Electric and magnetic field intensities of the multilayered nanostructure at the nickel middle plane for the minimum of reflectance ($\lambda = 616$ nm). The unit cell consisted of $L = 480$ nm, $D = 270$ nm, 50 nm thick Au layers and 70 nm Ni spacer.

5. Effective parameters retrieval of bianisotropic metamaterials

The effective properties of our samples were extracted from FDTD simulations and making use of the homogenization method.¹ This procedure is applied for asymmetric systems in the propagation direction, where the complex transmission and reflection coefficients, also known as S-parameters, differ depending on the side of illumination. As a result, two simulations have to be done for the retrieval of the effective constituents (Fig. S6a): one with the light coming from the top of the structure and one with the light coming from the bottom, which corresponds to the substrate in our case. Fig. S6b and c show the calculated amplitudes and phases of the S-parameters for the metamaterial exhibiting a refractive index of -1. Whereas the transmission curves present a similar behaviour due to reciprocity, the reflection amplitudes and phases differ and confirm the substrate-induced bianisotropy, in agreement with previous works.²

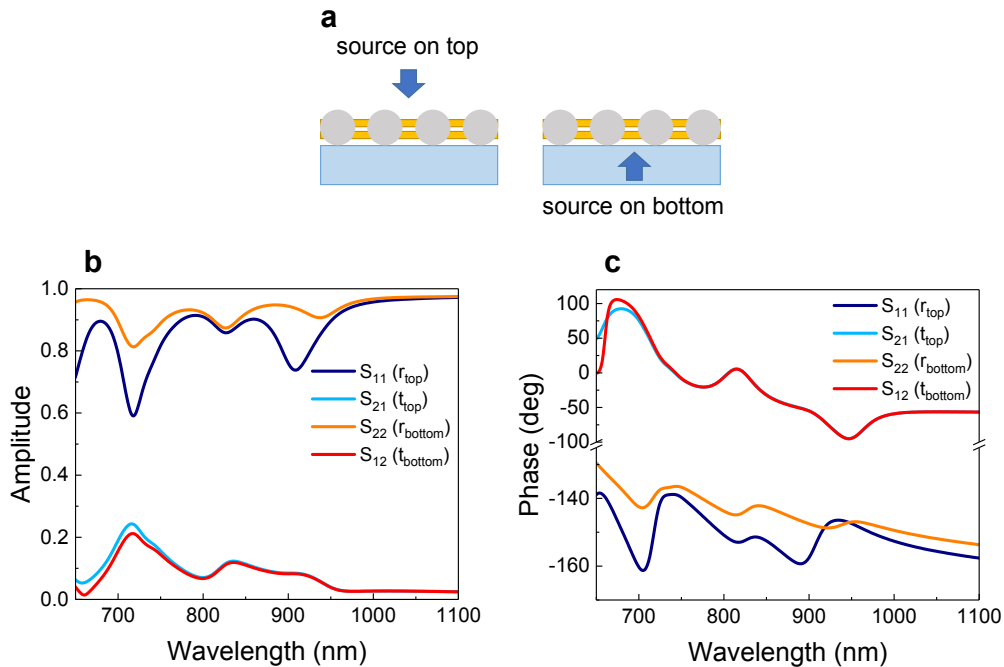


Fig. S6 (a) Schematic illustrations of the two simulations performed for the retrieval. (b) Amplitudes and (c) phases of the simulated S-parameters for the metamaterial exhibiting -1 refractive index,

where S_{11} and S_{21} denote the reflected and transmitted parameters with top incidence and S_{22} and S_{12} , the reflected and transmitted parameters with bottom incidence.

Having extracted the S-parameters for both directions, the effective properties were calculated according to the procedure reported by Li *et al.*³ The refractive index n was obtain from Eq. (1) and taking into account that for a passive medium the imaginary part must obey $n'' > 0$:

$$\cos(nkd) = \frac{1 - S_{11}S_{22} + S_{21}^2}{2S_{21}} \quad (1)$$

where k is the wave number of light in free space, d is the thickness of the metamaterial without involving the substrate, S_{11} and S_{21} are the reflection and transmission coefficients with top incidence, and S_{22} is the reflection coefficient with bottom incidence. Fig. S7 shows the real part of the retrieved refractive index for individual top and bottom incidences as well as the corrected effective value extracted from Eq. (1).

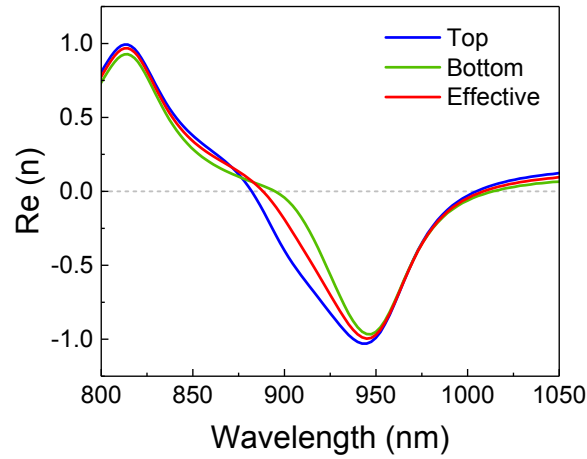


Fig. S7 Real part of the effective refractive indices when light comes from the top, from the substrate and the correction made considering both results.

Additionally, Fig. S8 presents the comparison of the effective refractive index for the same structure with and without substrate, showing that a free-standing membrane would exhibit a larger negative refractive index with a higher FOM. In all the cases, the correct choice of the branch from the cosine

function was verified using an alternative procedure based on the Kramers-Kronig dispersion relation,⁴ ensuring the validity of the retrieved parameters.

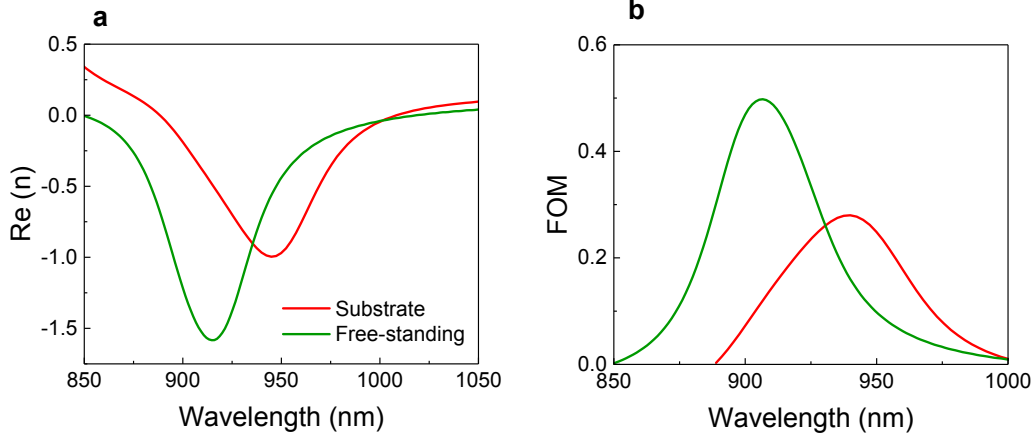


Fig. S8 (a) Real part of the effective refractive index and (b) figure of merit of the double fishnet metamaterial with and without substrate.

The magnetoelectric coupling, electric permittivity and the magnetic permeability were obtained from:

$$\xi = \left(\frac{n}{-2\sin(nkd)} \right) \left(\frac{S_{11} - S_{22}}{S_{21}} \right) \quad (2)$$

$$\mu = \left(\frac{in}{\sin(nkd)} \right) \left(\frac{2 + S_{11} + S_{22}}{2S_{21}} - \cos(nkd) \right) \quad (3)$$

$$\varepsilon = \frac{(n^2 + \xi^2)}{\mu} \quad (4)$$

For the impedance, two different values were obtained depending on the direction of the incoming light.

$$z^{\pm} = \frac{\mu}{n \pm i\xi} \quad (5)$$

6. Negative refraction in a metamaterial prism

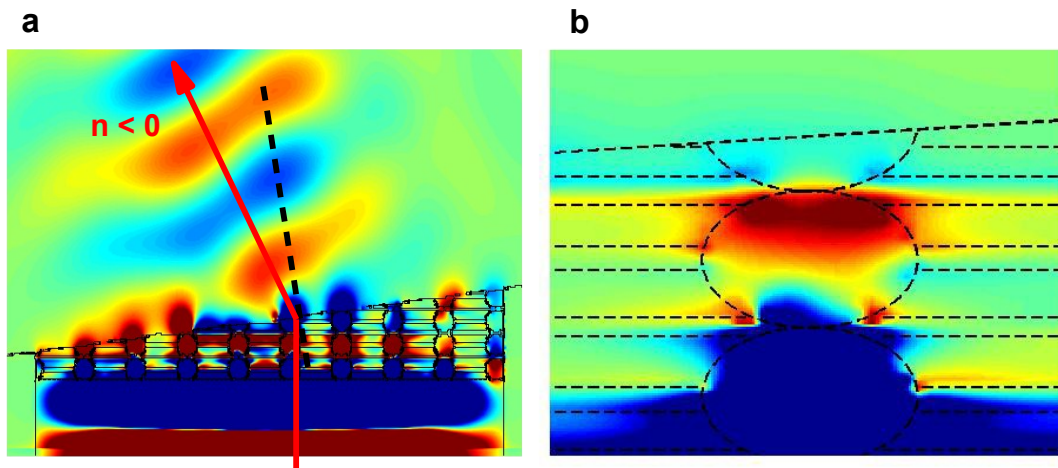


Fig. S9 Simulated electromagnetic behaviour of a prism composed of several layers of our fishnet metamaterial. (a) Electric field propagation at the wavelength of resonance showing negative refraction. (b) Magnified plot of the electric field distribution, where negative phase propagation occurs (see supplementary movies).

7. Angle dependence of the operation wavelength

The optical response of the metamaterial exhibiting a negative index of -1 has been numerically obtained for different angles of incidence for transverse magnetic (TM) and transverse electric (TE) polarizations. Fig. S11 shows how the resonance associated with the negative index, initially placed at 920 nm, shifts towards larger wavelengths as the angle of incidence increases.

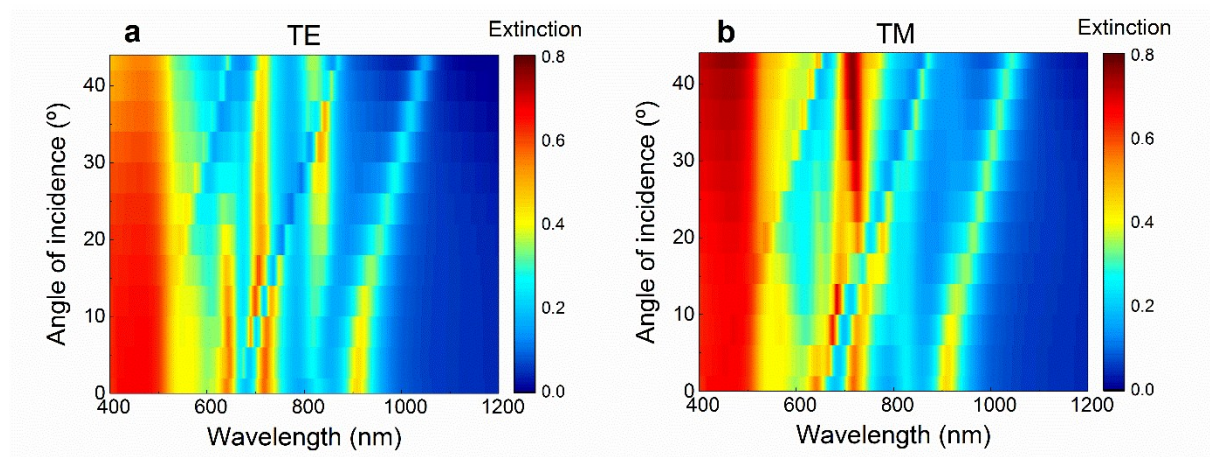


Fig. S10 Extinction versus wavelength and angle of incidence of the structure presenting a -1 refractive index for (a) TE and (b) TM polarizations.

8. Comparison between the experimental response and Fresnel modelling

In order to check the effective parameters of our samples, the reflection and transmission spectra were calculated for the simplest case where the metamaterial is replaced by a slab with the retrieved effective refractive index (Fig. S11a). Taking into account that in our case the magnetic permeability is $\mu \neq 1$, the reflection r and transmission t Fresnel coefficients for normal incidence will be:

$$r = \frac{r_{12} + r_{23}e^{2i\beta}}{1 + r_{12}r_{23}e^{2i\beta}} \quad (6)$$

$$t = \frac{t_{12}t_{23}e^{i\beta}}{1 + r_{12}r_{23}e^{2i\beta}} \quad (7)$$

where the propagation constant β inside the metamaterial is given by

$$\beta = \frac{2\pi}{\lambda}n_2 \quad (8)$$

and

$$r_{12} = \frac{\eta_1 - \eta_2}{\eta_1 + \eta_2} \quad (9)$$

$$t_{12} = \frac{2\eta_1}{\eta_1 + \eta_2} \quad (10)$$

being $\eta_i = \frac{1}{z_i} = \sqrt{\frac{\epsilon_i}{\mu_i}}$ the admittance, with analogous expressions for r_{23} and t_{23} .

Finally, the reflectance and transmittance will be given by:

$$R = |r|^2 \quad (11)$$

$$T = \frac{\eta_3}{\eta_1}|t|^2 \quad (12)$$

Figs. S11b-e present the extinction calculated *via* Fresnel equations compared to the experimental data of each sample and confirm the success of our effective parameters retrieval.

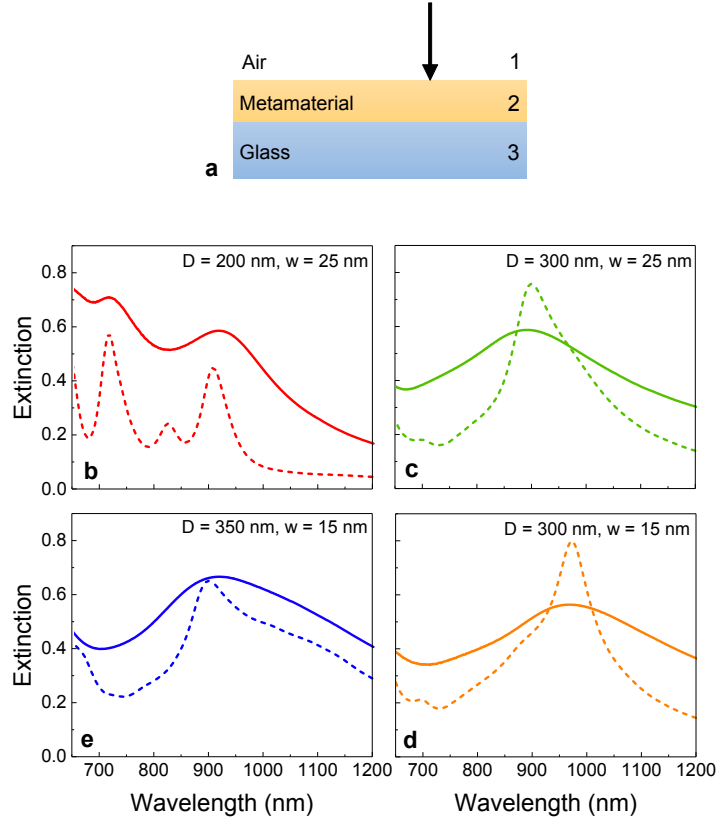


Fig. S11 (a) Schematic illustration of the effective system adopted for Fresnel modelling. Experimental (solid lines) and calculated (dashed lines) extinction spectra of samples with (a) $D = 200$ and $w = 25$ nm, (b) $D = 300$ nm and $w = 25$ nm, (c) $D = 300$ nm and $w = 15$ nm and (d) $D = 350$ nm and $w = 15$ nm.

9. Gap and diameter dependence of the negative refractive index

For two non-perforated gold films of thickness h separated by a gap width w , the gap-SPP dispersion relation in the low-frequency limit can be approximated by:

$$|k_{SPP}| = k_0 n_d \left[\frac{w}{w + 2\lambda_p \coth\left(\frac{2\pi h}{\lambda_p}\right)} \right]^{-1/2} \quad (13)$$

where k_0 is the vacuum wave number, n_d the refractive index of the dielectric spacer and λ_p would be the plasma wavelength of gold. Making some derivation the resonance wavelength λ can be expressed as:

$$\lambda^2 = A \left(1 + \frac{B}{w} \right) \quad (14)$$

where A and B are constants depending on the geometrical parameters and the material of the structure. Even though these dispersion equations are only valid for flat and continuous metallic layers, the dispersion when considering an array of holes perforating the films presents a similar dependence on w .⁵ It is therefore expected that the wavelength of resonance increases when decreasing w as our simulations illustrate (Fig. S12a). In the limit case when w is zero, the resonant circuit of the structure disappears and the magnetic resonance is lost, presenting a non-negative refractive index.

On the other hand, the electrical response of these structures is dominated by the cut-off wavelength λ_c of a circular hole waveguide:⁶

$$\lambda_c \approx \frac{\pi D}{1.841} n_{PS} \quad (15)$$

where n_{PS} is the refractive index of the polystyrene spheres of diameter D . Two regimes can be found concerning this value: (i) when $D > 175$ nm, λ_c is higher than the lattice parameter $L = 480$ nm and a decreasing of the diameter involves a more negative index as it is shown in Fig. 1b of the main text. (ii) On the contrary, when $D < 175$ nm ($\lambda_c < L$) the sphere size is so small that the output light does not effectively couple to the periodic structure. As a result, less negative values of the refractive index are obtained until reaching a diameter ($D = 100$ nm in our system) that does not perforate the gold slabs. In this case the refractive index of a simple gold film is recovered. This discussion is well confirmed by the simulations presented in Fig. S12b.

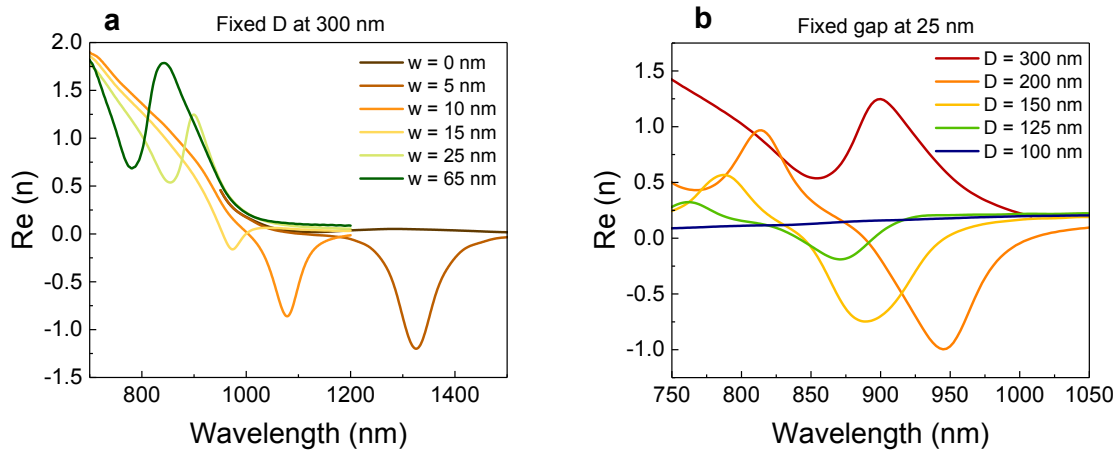


Fig. S12 Numerical simulations of the real part of the effective refractive index when varying (a) the air gap width between the gold layers of the spheres and (b) the diameter of the beads.

References

- 1 D. R. Smith, D. C. Vier, T. Koschny and C. M. Soukoulis, *Phys. Rev. E*, 2005, **71**, 036617.
- 2 S. Yun, Z. H. Jiang, D. Ma, Z. Liu, D. H. Werner and T. S. Mayer, *Appl. Phys. Lett.*, 2013, **103**, 233109.
- 3 Z. Li, K. Aydin and E. Ozbay, *Phys. Rev. E*, 2009, **79**, 026610.
- 4 Z. Szabo, G. Park, R. Hedge and E.-P. Li, *IEE Trans. Microw. Theory Tech.*, 2010, **58**, 2646–2653.
- 5 A. Mary, S. G. Rodrigo, F. J. Garcia-Vidal and L. Martin-Moreno, *Phys. Rev. Lett.*, 2008, **101**, 103902.
- 6 J. B. Pendry, L. Martin-Moreno and F. J. Garcia-Vidal, *Science*, 2004, **305**, 847–848.